International Journal of Engineering Innovation & Research
Volume 12, Issue 3, ISSN: 2277 – 5668

Principle and Experimental Study of Permanent Magnet Motor Drive Circuit

Fuqian Zhou[1], Hongbin Yin[1,2*], Peng Zhang[1], Congzhen Liu[1] and Wenjing Hu[1]
[1]School of Transportation and Vehicle Engineering, Shandong University of Technology, Shandong, Zibo, Zhangdian, 255049, China.
[2]China National Heavy Duty Truck Group Co. Ltd., Jinan 250013, China.
*Corresponding author email id: hbinyin@163.com

Date of publication (dd/mm/yyyy): 17/05/2023

***Abstract* – In the design process of permanent magnet motor hardware control system, there are some problems such as complicated drive circuit analysis and design and high time cost. In traditional three-phase current sampling, the process is complicated and the algorithm is difficult to implement. In this paper, the PS21A7A power chip as the core, based on the modular analysis design and test method, analysis of the permanent magnet motor drive circuit of the power supply circuit, power chip supply circuit, sampling circuit working principle and characteristics, reduce the complexity of circuit analysis and design. The three-resistance current sampling method is used to sample the phase current of the permanent magnet motor, which reduces the complexity of the control algorithm and improves the control precision of the system. The hardware circuit of the driving circuit is designed, and the driving control test of permanent magnet motor is carried out in combination with the Micro Lab Box main control unit.**

***Keywords* – Permanent Magnet Motor, Driving Circuit, Principle Analysis, Modular Analysis Design, Three-Resistance Sampling Method.**

I. INTRODUCTION

With the advantages of small size, light weight, high efficiency and high power density, permanent magnet motors are widely used in industrial control [1], new energy vehicles and many other fields [2]. As an important part of the motor drive control, the performance of the motor drive circuit directly affects the performance of the entire motor control system. In the analysis and design of motor drive circuits, the complexity of the circuit structure and principle makes the analysis and design process of drive circuits costly and time consuming, resulting in a significant reduction in circuit design efficiency. Therefore, fast and efficient drive circuit analysis and design has become one of the critical issues in the design of high-performance motor control system [3].

There are two types of drive for permanent magnet motors: square wave and sine wave, for permanent magnet brushless DC motors (BLDCM) and permanent magnet synchronous motors (PMSM) respectively [4]. The phase current of a permanent magnet brushless DC motor is similar to a square wave and the counter-electromotive force is similar to a trapezoidal wave. Hall sensors are usually required to detect the rotor position and make commutation judgements [5, 6]. The control circuit of a permanent magnet brushless DC motor is simple and the output torque is large. An inherent drawback of brushless DC motors is the pulsating phase change torque. This introduces a high level of noise, thus limiting its use in high precision and low noise applications [7, 8].

Wang Weiqiang [9] et al. designed a permanent magnet motor controller based on the STM32F103RBT6 chip, and carried out hardware circuit analysis and design. The three-phase current sampling used the single-resistance sampling method, which makes the control algorithm complex and increases the controller operating load; the modular design scheme was not applied to the hardware design, which is equally complex. Zhang Yang [10] et al. designed the control circuit, isolation circuit, drive circuit, inverter circuit and speed detection

circuit of the permanent magnet synchronous motor controller, using Hall current sensor to detect the three-phase current, which makes the cost of the controller increase and is not conducive to the application in practical engineering. In the literature [11, 12], permanent magnet brushless DC motor drivers were designed to improve the power factor and suppress current ripple. Sun [13] et al. designed the overall schematic, hardware and software for the digital control system of a permanent magnet synchronous motor, sampling Hall current sensors to detect phase currents in the closed-loop control of a permanent magnet motor, making the driver larger and more costly.

In response to the above problems, this paper proposes a modular analysis and design method for permanent magnet motor drive circuits, adopts the three-resistance current sampling method, designs a permanent magnet motor driver, tests the main functions of the permanent magnet motor driver, and the test results show that the studied motor driver can accurately and effectively implement permanent magnet motor control.

II. Permanent Magnet Motor Drive Circuit Analysis

The modular analysis and design method for permanent magnet motor drive circuits proposed in this paper is shown in Figure 1 and is classified according to the function of each part of the circuit in the permanent magnet motor drive circuit.

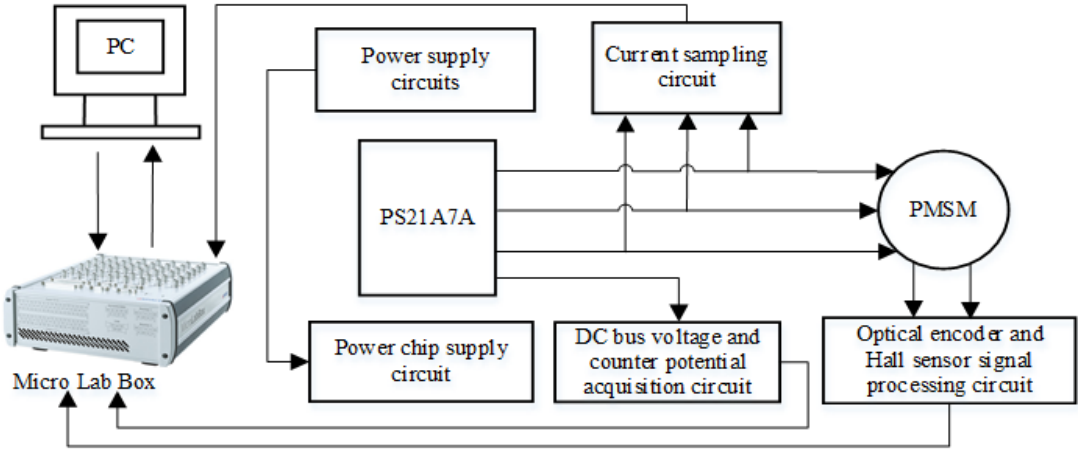

Fig. 1. Drive circuit modular scheme.

2.1. *Power Supply Circuit Analysis*

The drive circuit supports 24~48V (Max 60V) DC voltage input. The operating voltage of the PS21A7A power chip is 15V, and the operating voltage of the signal detection circuit and the protection circuit is 5V. Therefore, the power supply circuit needs to step down the input voltage twice. This paper; uses the LM7815 and LM7805 voltage regulator modules to step down the supply voltage. The regulator module contains over-current, over-temperature, and overload protection circuits. The ideal power supply should provide a stable DC voltage, but due to noise in the circuit, the circuit voltage will fluctuate and additional decoupling capacitors are required to make the circuit output voltage stable. When the regulator module cannot provide output current in time, the decoupling capacitor will compensate for the current, according to the compensation current calculation equation.

$$I = Ae^{j2\pi f_0 \frac{2r}{v_p}} = Ae^{j\pi \frac{4r}{Tv_p}} \quad (1)$$

Where A is the current amplitude; the exponential part is the compensating current phase; j is in imaginary units; f_0 is the self-resonant frequency of the capacitor; r is the distance of the voltage regulator module from the decoupling capacitor; v_p is the transmission speed of the compensating current signal.

In practical engineering applications where an ideal capacitor does not exist, a two-port impedance analyzer can be used to measure the actual resistance-frequency characteristic curve of the capacitor as shown in Figure 2.

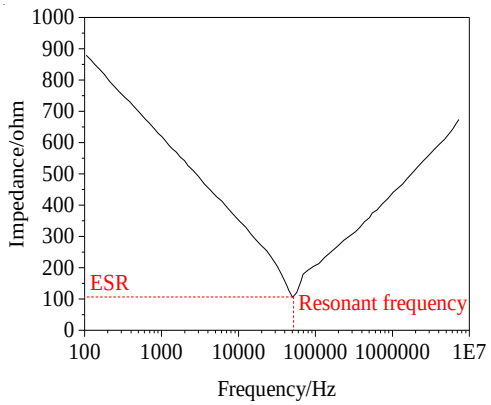

Fig. 2. Capacitor resistance frequency characteristic curve.

Electrolytic and ceramic capacitors are connected in parallel to achieve a decoupling effect, prevent sudden changes in power demand, and ensure the stability of the power supply. A Schottky diode with low power consumption is used to rectify the input voltage to prevent inrush currents. The schematic diagram of the power supply circuit is shown in Figure 3.

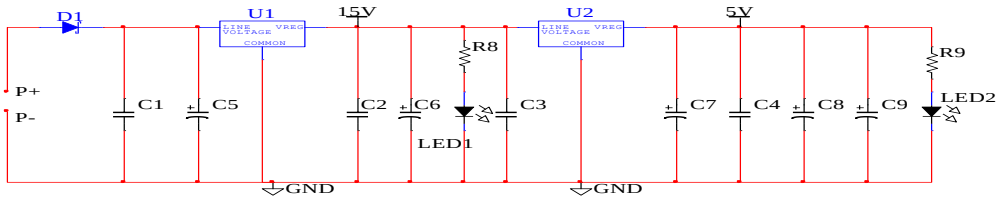

Fig. 3. Power supply circuit.

2.2. *Power Chip Supply Circuit Analysis*

The power chip U, V, W three-phase P-side drive power supply shall consist of three mutually independent power supplies, while the U, V, W three-phase N-side drive power supply must be a common power supply, so this paper will use a bootstrap circuit. The advantage of the bootstrap circuit is that the conventional power supply circuit required for the power chip module is replaced by a single power supply circuit, eliminating the need for three mutually isolated power supplies and making the structure simpler. When the power chip works normally, the IGBT in the power chip is in a saturated state, at which time the IGBT's through-state loss is minimal. According to the requirements for the normal operation of the power chip, the voltage of the power chip pins VUFB-VUFS, VVFB-VVFS and VWFB-VWFS should not exceed 20V, and the supply voltage in this paper is 15V. Three high-voltage drive modules and one low-voltage drive module are integrated inside the power chip; so that the drive supplies for each way are isolated from each other to avoid noise interference. D2, D3, and D8 are chosen as fast recovery (t_{rr}≤100ns) diodes to prevent current backflow, and D4, D5, and D6 are

voltage regulator diodes, working in the reverse breakdown zone. Resistors (R5, R6, R7) play the role of current limiting in the circuit to prevent excessive current from causing damage to the high and low-voltage driver-integrated modules. The power supply circuit of the power chip is shown in Figure 4.

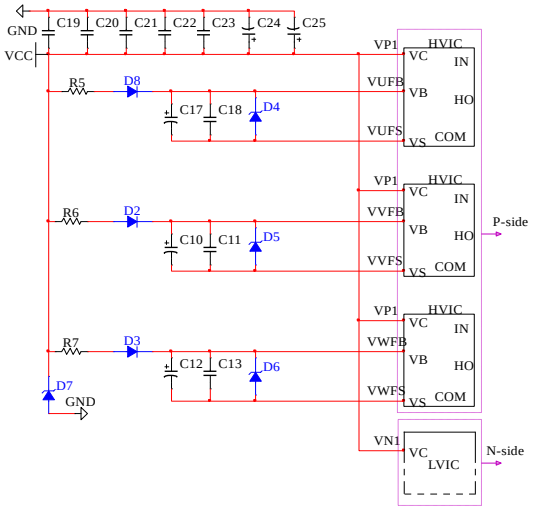

Fig. 4. Power chip supply circuit.

To meet the operating requirements of the power supply circuit of the power chip, the capacitors, resistors, and diodes in the circuit are calculated and selected. The calculation formula for the capacitor charging operating voltage is,

Charging process,

$$V_{VUFB} = V_{CC} - V_D - V_{sat} - I_D R_c \tag{2}$$

Stable state,

$$V_{VUFB} = V_{CC} \tag{3}$$

Where V_{CC} is the supply voltage; V_D is the forward voltage drop of the diode; V_{sat} is the saturation voltage drop across the power switch; I_D is the circuit current during charging; R_c is the resistance.

According to the power chip technical manual, capacitors C11, C13 and C18 are selected as ceramic capacitors with good temperature, frequency and bias characteristics, with capacitance values ranging from 0.22 to 2.0μF; capacitors C10, C12 and C17 are selected as electrolytic capacitors with good temperature and frequency characteristics. The capacitance value of the ceramic capacitor is 25V and 2μF, while the electrolytic capacitor is 25V and 100μF.

2.3. *Current Sampling Circuit Analysis*

In this paper, the motor phase current is collected by a three-resistor sampling method, which is based on connecting three detection resistors in series with the N-side IGBT emitter stage of the PS21A7A9 power chip, converting the collected motor phase current into a voltage drop, filtering it through the op-amp circuit, and amplifying the voltage drop signal to the main control unit A/D converter detection range, and further calculating the magnitude of the current through Ohm's law. The sampling resistors are R28, R29, and R30 and are connected as shown in Figure 5.

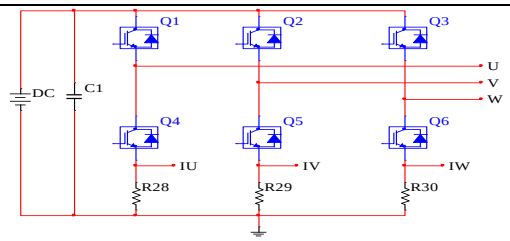

Fig. 5. Three-resistance current sampling method.

This paper uses an amplifier circuit consisting of the MCP6024, and the current sampling signal amplifier circuit is shown in Figure 6. When a positive signal is input from the in-phase input or a negative signal is input from the reverse input, the op-amp circuit has the effect of amplifying the DC signal, but when an AC signal is input, a negative signal is input at the in-phase end and a positive signal is input at the reverse end, the amplifier is not amplified because the emission junction will be reverse biased. Therefore, in order to obtain the correct AC amplification waveform, a DC bias voltage VREF is connected at the in-phase input, the size of which is half of the operating voltage VCC of the operational amplifier, so that the voltage at the in-phase input is greater than zero to access the amplifier circuit, while obtaining the maximum output dynamic response range.

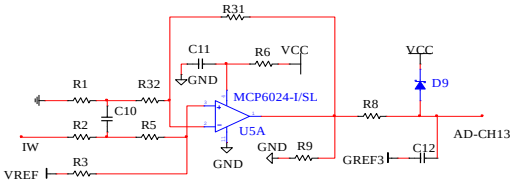

Fig. 6. Current sampling signal amplification circuit.

The voltage at the in-phase input AVCC is 3.3 V, so the DC bias voltage V_{REF} is 1.65 V. The circuit is an in-phase proportional arithmetic circuit with an amplification formula.

$$A_u = \frac{R_{31}}{R_{32}} + 1 \tag{4}$$

Assuming that the sampling port I_W phase voltage is U_{IW}, the amplifier circuit output port voltage signal $U_{AD\text{-}CH13}$ is,

$$U_{AD-CH13} = U_{IW} A_u + V_{REF} \tag{5}$$

The current flowing through the three-phase load is,

$$i = \frac{U_{AD-CH13} - V_{REF}}{A_u R} \tag{6}$$

2.4. *Bus Voltage and Counter Potential Collection Circuit Analysis*

In this paper, the end voltage method is used to collect the counter-electromotive force, the collection circuit should have resistive voltage divider and RC low-pass filtering processing function, the end voltage amplitude will be limited to the normal operating voltage range of the detection voltage, and the high frequency part of the end voltage will be filtered out to make the collection signal more accurate, the voltage divider circuit is used for voltage divider processing, the voltage signal is connected to the control unit, the counter-electromotive force collection circuit is shown in Figure 7.

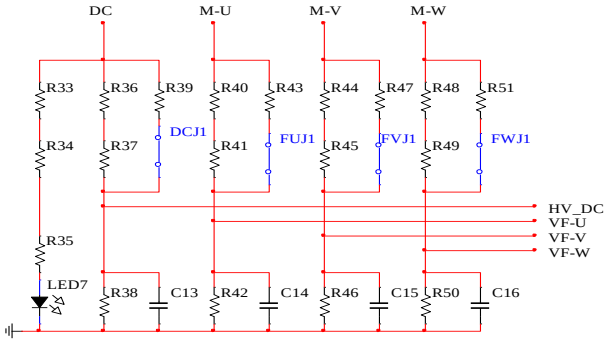

Fig. 7. DC bus voltage and counter-electromotive force collection circuit.

The circuit uses a Jump wire for the collection of signals in different operating conditions at low voltage and high voltage. When the power supply voltage is 24V, DCJ1 is shorted, and according to the circuit voltage division principle and Ohm's law, the test port output voltage formula.

$$u_{dc1} = \frac{R_{38}(R_{36} + R_{37} + R_{39})U_{DC}}{(R_{39} + R_{38})(R_{36} + R_{37}) + R_{38}R_{39}} \tag{7}$$

Where u_{dc1} is the DC bus voltage test voltage at low voltage; U_{DC} is the DC bus voltage. When DCJ1 is disconnected during high-voltage operation, the output voltage of the test port is,

$$u_{dc2} = \frac{R_{38}}{R_{36} + R_{37} + R_{38}} U_{DC} \tag{8}$$

Where u_{dc2} is the DC bus voltage test voltage at high voltage. Using the above method, the signal voltage value at the output of the counter-electromotive force collection circuit can also be calculated.

2.5. *Optical Encoder and Hall Sensor Signal Processing Circuit Analysis*

The Hall sensor signal processing circuit is shown in Figure 8. R55, R56 and R57 form an RC filter circuit with C18, C19 and C20 respectively, R52, R53 and R54 are pull-up resistors, and HALL-A, HALL-B and HALL-C are connected to the control unit for detection.

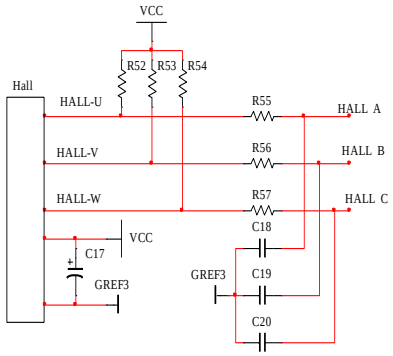

Fig. 8. Hall sensor signal conditioning circuit.

The optical encoder signal processing circuit is shown in Figure 9, in which R58 and C21, R59 and C22, and R60 and C23 form a first-order filter circuit, and the RC filter circuit cut-off frequency is,

$$f_p = \frac{1}{2\pi RC} \tag{9}$$

Where f_p is the filter circuit cut-off frequency, the cut-off frequency of this RC filter circuit is approximately 1.05kHz. R61, R62, and R63 are pull-up resistors, that filter out high-frequency signal interference. A 10uF capacitor is connected between the positive and negative terminals of the encoder power supply to remove noise from the supply side and prevent it from interfering with the output signal of the encoder.

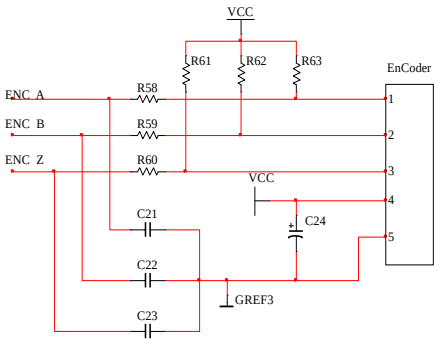

Fig. 9. Photoelectric encoder signal conditioning circuit.

III. TEST VERIFICATION

In order to verify the effectiveness and accuracy of the circuits studied in this paper, tests were carried out based on the Micro Lab Box master control unit. The PMSM control test bench is shown in Figure 10 and the parameters of the permanent magnet motor control system are shown in Table 1. The Micro Lab Box master control unit is the hardware system of a semi-physical simulation platform developed by the German company dSPACE. dSPACE is based on the control system design software MATLAB/Simulink and is fully compatible with MATLAB/Simulink, which is the mainstream semi-physical simulation platform for Rapid Control Prototyping (RCP) test.

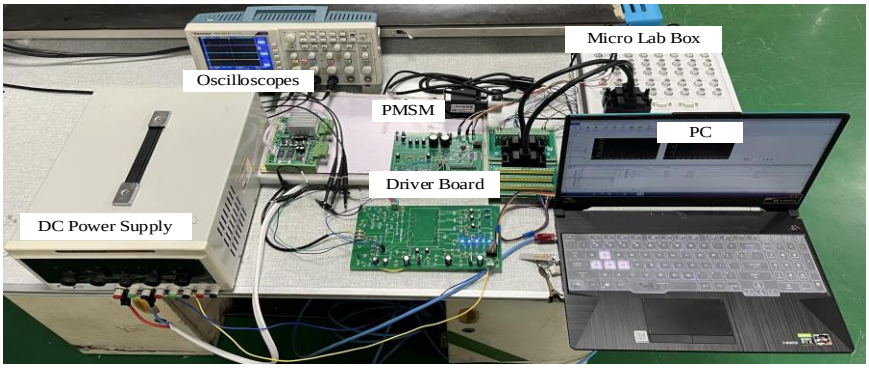

Fig. 10. PMSM control test bench.

Table 1. Permanent magnet motor control system parameters.

Parameters	Value	Parameters	Value
Rated Power/W	62	Stator Resistance/Ω	0.89
Rated Voltage/V	24	Inductance/mH	0.62
Rated Current/A	4.0	Number of Pole Pairs	4
Peak Current/A	14	Permanent Magnet Flux Linkage/Wb	0.005515
Rated Speed (r/min)	3000	EMF Constant/(V/Krpm)	4.0

Parameters	Value	Parameters	Value
Rated Torque/ (N·m)	0.2	DC Bus Voltage/V	24
Peak Torque/ (N·m)	0.7		

The input of the power supply circuit is connected to a voltage of 18V~30V, and the actual output voltage value of the power supply circuit is measured by a multimeter as shown in Table 2.

Table 2. Experimental results of power supply circuit.

Input Voltage/V	**Main Buck Circuit Output Voltage**/V	**Secondary Buck Circuit Output Voltage**/V
18	15.04	4.95
20	15.06	4.95
22	15.06	4.95
24	15.05	4.95
26	15.06	4.95
28	15.07	4.95
30	15.07	4.95

The output voltage range of the main buck circuit is 15.04V~15.07V and the output voltage of the secondary buck circuit is 4.95V. Using 15V and 5V as reference values, the maximum output voltage error of the main buck circuit is calculated to be 0.467% and the maximum output voltage error of the secondary buck circuit is 1.0%, so the output voltage of the power supply circuit is stable and the output results meet the actual requirements.

By testing the VUFB, VVFB and VWFB terminals of the power supply circuit of the power chip, the voltage waveform of the circuit was obtained as shown in Figure 11, with a voltage value of 15V. It can be seen from the testing waveform that the voltage value is stable and can provide the required voltage value for the normal operation of the high and low voltage drive integrated modules of the power chip.

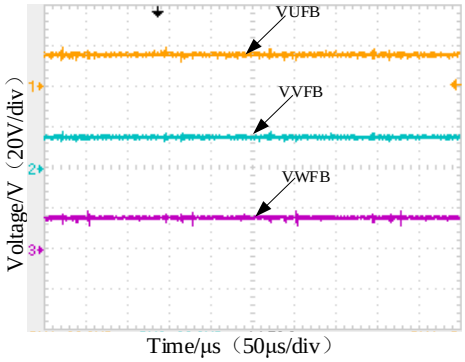

Fig. 11. Power chip supply circuit voltage.

The voltage waveform shown in Figure 12 is obtained by detecting the voltage at the output of the current sampling circuit, with a voltage amplitude of approximately 1.2V. The collected signal waveform is stable, and the actual three-phase motor current waveform shown in Figure 13 is obtained after A/D conversion by the Micro Lab Box master control unit, with a current amplitude of approximately 2.7A.

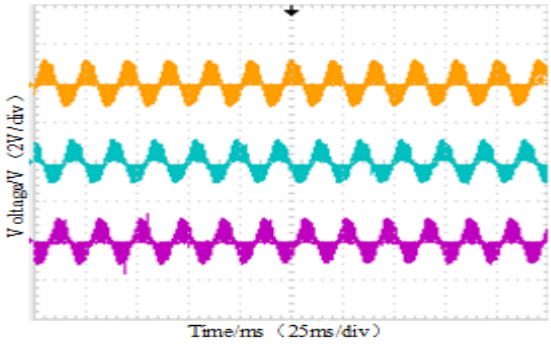

Fig. 12. Current sampling circuit output waveform.

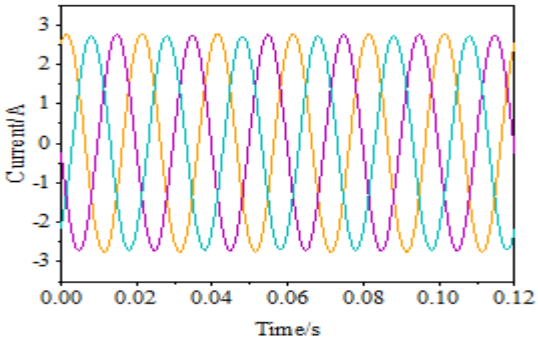

Fig. 13. PMSM current waveform.

The motor speed curve and motor rotor position curve are shown in Figure 14. The motor reference speed is 750r/min and the maximum error of the actual motor speed is 1.67%. The motor speed fluctuation is small, indicating that the hardware circuit can meet the performance index requirements.

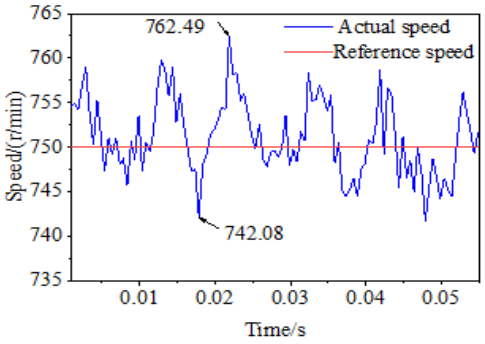

Fig. 14. PMSM speed curve.

IV CONCLUSION

This paper presents a modular analysis and design method for permanent magnet motor driver circuit, which reduces the time cost of designing permanent magnet motor driver. The working principle and characteristics of the permanent magnet motor power supply circuit, power chip power supply circuit and sampling circuit are analyzed. Through the design of the hardware circuit, the driving circuit of the permanent magnet motor is tested and verified.

(1) A new modular analysis model of permanent magnet motor drive circuit is proposed, as shown in Figure 1. According to the function of each part of the drive circuit, it is divided into power supply circuit, power chip supply circuit, current sampling circuit, bus voltage and back potential acquisition circuit, photoelectric encoder and Hall sensor signal processing circuit.

(2) A modular analysis and design of the power supply circuit in the permanent magnet motor drive circuit was carried out. The LM7815 and LM7805 voltage regulator chips are used as the power circuit voltage regulator module to achieve an average output voltage of 15.06V and 4.95V, when the DC input voltage is 18V-30V. Based on the operating characteristics of the PS21A7A power chip, the power chip supply circuit is analysed. The voltage output of the power supply circuit and the power chip supply circuit is stable and meets the actual requirements.

(3) In order to achieve real-time acquisition of the three-phase current of the permanent magnet motor, the thre-

-e resistance sampling method is used for current acquisition, and the current signal is amplified by the op amp circuit so that it can reach the voltage value identified by the main control unit, and the actual three-phase current amplitude of the motor is finally obtained as 2.7A. The three-resistance sampling method reduces the difficulty of the algorithm and improves the sampling accuracy. The Hall sensor and photoelectric encoder signal conditioning circuit is analysed, and the maximum error of motor speed fluctuation is 1.67% to achieve accurate control of the permanent magnet motor.

ACKNOWLEDGEMENT

This work was supported in part by the Natural Science Foundation of Shandong Province under Grant ZR2020QE155, in part by the Key R&D Project of Shandong Province under Grant 2019JZZY020112, and in part by the Key Laboratory of Precision Manufacturing and Special Processing of Shandong Province under Grant 9001-5322019.

REFERENCES

[1] Zhang Z.R., Wang D., Hua W. Overview of configuration, Design and control technology of hybrid excitation machines [J]. Proceedings of the CSEE, 2020, 40(24): 7834-7850+8221.
[2] Ding R.J., Liu K. future perspective for key technologies of motor drive system of new energy vehicles [J]. Chinese Engineering Science, 2019, 21(3):56-60.
[3] Guancheng X., Miao L., Xiangjun M., et al. Analysis of influence of insulation failure of drive transformer on drive circuit of SiC MOSFET[C]//2021 11th International Conference on Power and Energy Systems (ICPES). IEEE, 2021: 240-243.
[4] Woo J.H., Jung D.H., Choi J., et al. A study on IPMSM design, as the load motor for the motor driving test of urban railway vehicle through HILS, for achieving high power density [C]// 2016 19th International Conference on Electrical Machines and Systems (ICEMS). IEEE, 2016: 1-4.
[5] Morimoto S, Sanada M, Takeda Y. Wide-speed operation of interior permanent magnet synchronous motors with high-performance current regulator[J]. IEEE Transactions on Industry Applications, 1994, 30(4): 920-926.
[6] Qi H, Ling L, Li-kun X, et al. Research on the characteristics of open winding brushless DC motor[C]//2019 22nd International Conference on Electrical Machines and Systems (ICEMS). IEEE, 2019: 1-6.
[7] Liu L, Zhao M, Yuan X, et al. Direct instantaneous torque control system for switched reluctance motor in electric vehicles[J]. The Journal of Engineering, 2019, 2019(16): 1847-1852.
[8] Huang Q, Luo L, Zhang Y, et al. Commutation torque ripple suppression in three phase brushless DC motor using open-end Winding [J]. International Journal of Control, Automation and Systems, 2021, 19(8): 2747-2758.
[9] WANG Weiqiang, ZENG Xiaosong, XIA Maoshu. Design of permanent magnet brushless DC motor controller for electric vehicle [J]. Journal of Huaqiao University (Natural Science), 2019, 40(01):20-25.
[10] Fan Z., Wan Z., Yang Z., et al. Design and simulation of permanent magnet synchronous motor controller for twin oar electric boat [C]//2021 2nd International Conference on Computer Engineering and Intelligent Control (ICCEIC). IEEE, 2021: 138-142.
[11] Yu ZA, Ge TY, Liang JW Design of high power factor brushless DC motor [J]. Manufacturing Automation, 2019, 41(04): 91-95+ 105.
[12] WANG Qijun, YANG Kun, SU Zhanbiao, YANG Feng. Design of BLDC motor driver based on hardware FOC. Transducer and Microsystem Technologies, 2021,40(06):89-91+94.
[13] Chen L., Sun X., Wang S, et al. Digital control system design for bearing less permanent magnet synchronous motors [J]. Bulletin of the Polish Academy of Sciences: Technical Sciences, 2018: 687-698-687-698.

AUTHOR'S PROFILE

First Author
Fuqian Zhou, Male, Master's in reading, School of Transportation and Vehicle Engineering, Shandong University of Technology, Shandong, Zibo, Zhangdian, 255049, China. He received the B.S. degree in vehicle engineering from the Shandong University of Technology, Zibo, China, in 2021. email id: zfq19862519716@163.com

Second Author
Hongbin Yin, Male, Lecturer, School of Transportation and Vehicle Engineering, Shandong University of Technology, (Correspondence author), Shandong, Zibo, Zhangdian, 255049, China. Received M.S. degree in power machinery and engineering from the Shandong University of Technology, Zibo China, in 2012, and received Ph.D. degree in vehicle engineering from the Jilin University, Changchun, China, in 2019. From 2015 to 2019, he has been with the College of Automotive Engineering, Jilin University, Changchun, China, where he was involved in various research projects. He is also with the China Automotive Technology and Research Center Co., Ltd., as Intern Engineer. His research interests include the control and modeli-ng of electrical drives, the design of electric machines, and automotive applications of electric motor drives.

Third Author
Peng Zhang, Male , Master's in reading, School of Transportation and Vehicle Engineering, Shandong University of Technology, Shandong, Zibo, Zhangdian, 255049, China. He received the B.S. degree in automobile service engineering from the Qilu University of Technology, Jinan, China, in 2020.

Fourth Author
Congzhen Liu, Male, Doctor of Engineering, Associate professor, School of Transportation and Vehicle Engineering, Shandong University of Technology, Shandong, Zibo, Zhangdian, 255049, China. email id: lcz200811@163.com

Fifth Author
Wenjing Hu, Doctor of Engineering, lecturer, School of Transportation and Vehicle Engineering, Shandong University of Technology, Shandong, Zibo, Zhangdian, 255049, China. email id: huwenjing@sdut.edu.cn